

# Nightjar: Dynamic Adaptive Speculative Decoding for Large Language Models Serving

Rui Li, Zhaoning Zhang, Libo Zhang, Huaimin Wang, Xiang Fu, Zhiquan Lai  
 State Key Laboratory of Complex & Critical Software Environment  
 National Key Laboratory of Parallel and Distributed Computing  
 College of Computer Science and Technology, National University of Defense Technology  
 Changsha, China

**Abstract**—Speculative decoding (SD) accelerates LLM inference by verifying draft tokens in parallel. However, this method presents a critical trade-off: it improves throughput in low-load, memory-bound systems but degrades performance in high-load, compute-bound environments due to verification overhead. Existing Speculative Decoding strategies typically rely on static speculative lengths, failing to adapt to fluctuating request loads or identify the optimal moment to halt speculation. The cost of restarting speculative inference also remains unquantified. During traffic surges, the marginal utility of speculation diminishes; yet, the draft model’s persistent memory footprint competes for available KV cache. This resource contention limits the maximum batch size, thereby degrading overall system throughput. To overcome this, we propose Nightjar, a resource-aware adaptive speculative framework. It first adjusts to the request load by dynamically selecting the optimal speculative length for different batch sizes. Crucially, upon detecting significant request queuing or KV cache shortages, it disables speculative decoding and offloads the draft model to the CPU. This reclaims memory for the KV cache, thereby facilitating larger batch sizes and maximizing overall system throughput. Experiments show that Nightjar achieves up to 27.29% higher throughput and 12.90% lower latency compared to standard speculative decoding under dynamic request arrival rates in real-time LLM serving scenarios.

**Index Terms**—Speculative decoding, Large language models serving, Resource Efficient Inference, Dynamic real-time request loads

## 1. Introduction

Large language models (LLMs) are increasingly deployed in real-world applications, where they serve concurrent requests with varying throughput requirements. However, the LLM serving system faces high latency and low throughput due to the sequential nature of autoregressive decoding and the limited memory of the GPU [1].

Speculative decoding (SD) [2], [3] accelerates inference by allowing a draft model to propose multiple candidate

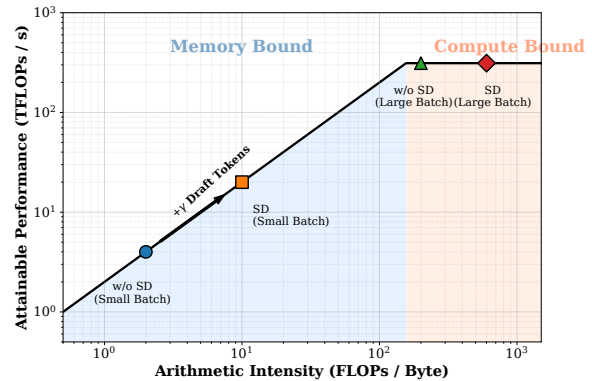


Figure 1. Conceptual Roofline model illustrating the performance shift in LLM inference between standard autoregressive decoding (w/o SD) and speculative decoding (SD); positions are illustrative.

tokens, while the target model verifies them in parallel, which is theoretically lossless in terms of accuracy. This reduces the strictly sequential dependency in autoregressive decoding and increases concurrency. From a roofline perspective (Figure 1), under small batch sizes, speculative decoding raises arithmetic intensity by verifying multiple draft tokens per weight, enhancing utilization in the memory-bound regime. As batch size increases, compute demands dominate and the speculative verification overhead pushes the system into the larger compute-bound region, diminishing speculative gains, whereas traditional autoregressive decoding scales more efficiently and increases throughput.

However, current speculative decoding implementations (e.g., in vLLM [4]) often use a fixed speculative length, which is not optimal for dynamic request loads. The optimal speculative length is a dynamic variable dictated by the interplay of batch size, token acceptance rates, and hardware characteristics. An excessively long speculative length increases the time spent on draft generation and imposes significant verification overhead, whereas a length that is too short fails to fully capitalize on the potential speedup of speculative decoding. Crucially, an effective system must decisively disable speculation when its marginal benefits vanish.

Furthermore, model-based draft models consume both

compute resources and precious GPU memory, unlike model-free approaches such as N-gram that incur negligible memory footprints. However, model-free methods lack generalizability and are often restricted to specific domains like code generation [5]. In high-traffic scenarios, the memory occupied by these draft models directly competes with the KV cache; reclaiming this space for the KV cache would facilitate larger batch sizes and significantly maximize overall system throughput.

Most optimizations for speculative decoding ignore the volatility of real-world serving. Early works targeted single requests [6], [7], [8], [9], [10] or static batches [11], [12], making them unsuitable for fluctuating traffic. Newer dynamic approaches [11], [13], [14], [15] also have flaws. For example, SpecServe [14] and TETRIS [16] rely on draft confidence, which scales poorly with large batch sizes. DSD [13] adjusts length based on historical acceptance rates. This creates a 'deadlock': if speculation is turned off, data collection stops, trapping the system in a suboptimal state. Even BanditSpec [12], which introduced Multi-Armed Bandits, uses a static design that is incompatible with the continuous batching of modern systems.

While existing works such as Oneiros [17] and eLLM [18] attempt to optimize GPU memory through memory remapping or shared pools, they predominantly focus on general-purpose memory management within or across models. Consequently, they overlook the tight coupling between strategic policy decisions (e.g., speculative length) and memory allocation (e.g., the residency of the draft model) inherent in the speculative decoding paradigm.

Therefore, the field urgently needs a truly intelligent, adaptive decision-making mechanism that can perceive load changes in real-time and accurately weigh the trade-offs between benefits and costs. It must be capable of dynamically selecting the optimal speculative strategy for different batch sizes at each decoding step, including decisively disabling it when necessary. To address this core challenge, we propose **Nightjar**, a contextual bandit approach for speculative length selection in dynamic, real-time LLM services. A key feature of our approach is its ability to learn the optimal speculative length for different batch sizes at each decoding step, without requiring prior knowledge of request difficulty or model characteristics. Furthermore, we incorporate the switching cost of transitioning from a speculative length of 0 to a positive value, a factor previously overlooked. By dynamically offloading the draft model upon disabling speculative inference, we reclaim substantial memory for the KV cache, thereby facilitating larger batch sizes and maximizing overall system throughput. Simultaneously, when a reduction in request load is detected, we proactively and asynchronously reload the draft model to re-enable speculative decoding, ensuring sustained performance gains. Implemented on vLLM [4] and evaluated on three real-world datasets, Nightjar significantly accelerates LLM inference, establishing a new state-of-the-art. It consistently outperforms existing methods, achieving an average throughput improvement of 27.29% over the vanilla baseline and 7.39% over the strongest existing method. Coupled with up to

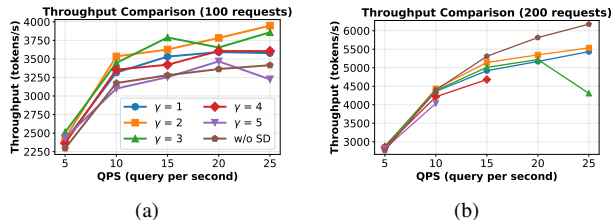


Figure 2. Throughput under different request loads and rates.  $\gamma$  denotes the speculative length (tokens generated by the draft model per step). Note: Configurations with  $\gamma \geq 4$  are omitted at high QPS due to GPU out-of-memory (OOM) errors.

12.90% lower latency compared to standard speculative decoding, these results demonstrate Nightjar’s practical effectiveness for dynamic and real-time LLM serving.

## 2. Motivation

Although modern LLM serving systems, e.g., vLLM [4], have been widely adopted in production, challenges remain in achieving high throughput and low latency with speculative decoding.

### 2.1. Dynamic Speculative Decoding Length Selection

In speculative decoding, the draft model generates  $\gamma$  tokens, which are subsequently verified by the target model in parallel. Consequently, the total latency per iteration is the sum of the draft model’s generation time and the target model’s verification time. The actual number of tokens produced per step equals the number of accepted tokens ( $n$ ) plus one bonus token. While increasing the speculative length  $\gamma$  can potentially raise the number of accepted tokens, it also incurs a higher temporal cost. If the acceptance rate (the ratio of accepted tokens to  $\gamma$ ) is low, the added overhead may outweigh the gains, ultimately leading to a decrease in overall throughput.

We empirically validate this trade-off<sup>1</sup>. As shown in Figure 2(a), SD provides significant speedups at lower request loads. For instance, a speculative length ( $\gamma$ ) of 3 improves throughput by 15.5% at 15 QPS while a speculative length of 2 yields better improvement than 3 at QPS=25. However, as the load increases, Autoregressive (AR) decoding surpasses SD’s performance. At high loads (Figure 2(b)), the overhead becomes detrimental, leading to a performance degradation of up to 30.25% compared to AR. This confirms that SD excels in the memory-bound regime, while its verification overhead becomes a liability when the system is compute-bound.

The core challenge lies in the dynamic and unpredictable nature of real-world LLM serving loads. Consequently, a

1. Experiments were conducted on the ShareGPT dataset using vLLM with the DeepSeek-R1-Distill-Qwen-7B model and a 0.5B draft model [19] on an RTX 4090 GPU.

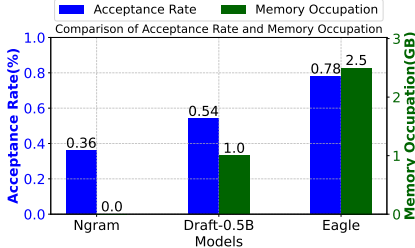


Figure 3. Memory occupation for different draft methods.

fixed speculative length is inherently suboptimal, as a configuration tuned for low-load efficiency can degrade service under high traffic. The optimal speculative length is not a static value but a dynamic variable dependent on real-time factors like system load, hardware characteristics, and token acceptance rates [20].

## 2.2. Memory underutilization

TABLE 1. KV CACHE MEMORY OCCUPATION FOR DIFFERENT MODELS.

| Context Length | Vicuna-13B | DeepSeek-R1-Distill-Qwen-7B |
|----------------|------------|-----------------------------|
| 1,024 (1K)     | 800 MiB    | 56 MiB                      |
| 4,096 (4K)     | 3,200 MiB  | 224 MiB                     |
| 8,192 (8K)     | 6,400 MiB  | 448 MiB                     |
| 32,768 (32K)   | 25,600 MiB | 1,792 MiB                   |

As evidenced by Table 1, the memory footprint of the KV cache is not only substantial but scales aggressively with context length, transitioning from a negligible overhead to a primary consumer of GPU resources. This expansion creates a zero-sum competition within the finite memory budget: as the KV cache encroaches upon the available memory, it directly constrains the headroom for resident draft model weights. Such resource contention highlights a critical bottleneck in static memory partitioning, where the burgeoning cache demands can eventually marginalize auxiliary models and degrade overall system throughput.

As shown in Figure 3, draft models (Ngram, DeepSeek-R1-DRAFT-Qwen2.5-0.5B [19], Eagle [21]) occupy varying GPU memory, impacting KV cache capacity. While their weights are smaller than the main model, they constrain memory under high loads. This memory overhead is particularly critical for large-scale models. Consider a standard deployment of DeepSeek-V3 671B [22] across  $10 \times H100$  (80GB) GPUs. The 14B MTP draft model, distributed via tensor parallelism, consumes 1.4GB of HBM per GPU. Under the MLA architecture [22], this specific memory slice is extremely valuable, equivalent to the storage of  $\sim 49k$  KV cache tokens. Current systems (e.g., vLLM [4]) retain draft models even when SD is disabled, wasting memory.

Fundamentally, we identify that this memory inefficiency arises from the isolation of weight and KV cache spaces in existing systems. This isolation hinders the dynamic redistribution of memory resources based on work-

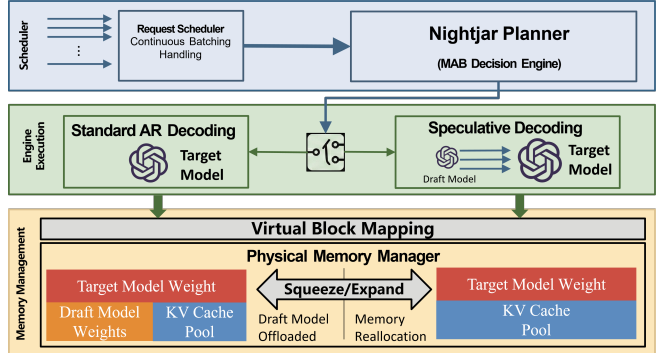


Figure 4. The Nightjar architecture operates across three layers: (1) The **Scheduler** manages incoming requests; (2) The **Planner** makes step-wise decisions to toggle speculation; (3) The **Memory Manager** dynamically reallocates resources between model weights and the KV cache pool based on system load.

load demands, leading to underutilized activation memory, which exacerbates KV cache space pressure and ultimately constrains overall system performance.

## 3. System Architecture

As illustrated in Figure 4, Nightjar is designed as a vertically integrated framework that coordinates decision-making across three functional layers: the Scheduler, Engine Execution, and Memory Management.

**1) Scheduler and Planner Layer.** At the top level, the *Request Scheduler* handles continuous batching for incoming requests. It feeds real-time batch statistics (e.g., current batch size  $B$ ) to the **Nightjar Planner**, which employs a Contextual Multi-Armed Bandit (MAB) engine to determine the optimal speculative length  $\gamma$  for the current decoding step.

**2) Engine Execution Layer.** Driven by the Planner’s decision, the execution engine dynamically switches between two modes:

- *Speculative Decoding (Right):* When the Planner selects  $\gamma > 0$ , the system engages the draft model to propose tokens, which are verified in parallel by the target model.
- *Standard AR Decoding (Left):* If the Planner selects  $\gamma = 0$ , speculation is disabled. The system bypasses the draft model entirely to avoid verification overhead.

**3) Memory Management Layer.** Underlying the execution is an elastic Memory Manager. As shown in the bottom panel of Figure 4, this module manages the contention between draft model weights and the KV cache. It implements a “Squeeze/Expand” mechanism: when the speculative decoding is disabled and memory is insufficient for the KV cache, it offloads the draft model to host memory to expand the KV cache pool, maximizing batch size. Conversely, during low load, it reallocates memory to reload

the draft model before re-enabling speculative decoding, ensuring accelerated inference.

This hierarchical design allows Nightjar to adapt to fluctuating workloads at both the algorithmic level and the system level.

## 4. Multi-Armed Bandit for Speculative Length Selection

In this section, we introduce the multi-armed bandit (MAB) for speculative length selection.

### 4.1. Problem Statement

In continuous batching [4] for LLM serving, the batch size can vary at each decoding step. We consider batch sizes  $B \in \mathcal{B} = \{1, 2, \dots, B_{\max}\}$  and speculative lengths  $\gamma \in \{0, 1, \dots, \Gamma_{\max}\}$ . While performance is often evaluated using *goodput*  $g_{B,\gamma}$  (tokens/sec), directly maximizing goodput ignores the heavy latency overhead caused by KV cache reconstruction during strategy switches.

To explicitly account for this cost, we formulate the problem as minimizing the *latency per token*, denoted as  $\ell_{B,\gamma} = 1/g_{B,\gamma}$ . Our objective is to select, for each batch size  $B$ , the speculative length  $\gamma$  that minimizes the effective latency:

$$\gamma^*(B) = \arg \min_{\gamma \in \{0, 1, \dots, \Gamma_{\max}\}} \ell_{B,\gamma} \quad (1)$$

Since the token acceptance rate is unknown a priori, we model this as a regret minimization task over  $T$  steps. We define the **Loss** observed at step  $t$ , denoted as  $L_t(\gamma)$ , to be the realized latency per token plus the switching overhead:

$$L_t(\gamma) = \ell_{B,\gamma_t}^t + \mathbb{I}(\gamma_{t-1} = 0 \wedge \gamma_t > 0) \cdot \frac{C_{\text{switch}}}{\gamma_t} \quad (2)$$

where  $\ell_{B,\gamma_t}^t$  is the observed inverse goodput,  $\mathbb{I}(\cdot)$  is the indicator function for a strategy switch, and  $C_{\text{switch}}$  is the latency overhead of KV cache reconstruction amortized over the generated tokens.

The cumulative regret  $R(T)$  is defined as the difference between the total loss incurred by the algorithm and the loss of the optimal fixed policy  $\pi^*$  that knows the true distributions:

$$R(T) = \sum_{t=1}^T (L_t(\gamma_t) - L_t(\gamma^*)) \quad (3)$$

Our goal is to find a policy that minimizes  $R(T)$ . We summarize the key notations and their descriptions in Table 2.

### 4.2. Algorithm Design

Contextual MAB can take dynamic request batch size or input sequences as context, such as linear Thompson [23] or LinUCB [24], which have been successfully applied in online prediction settings like configuration selection [25].

TABLE 2. SUMMARY OF KEY NOTATIONS USED IN NIGHTJAR.

| Symbol                                                | Description                                                                                                                                     |
|-------------------------------------------------------|-------------------------------------------------------------------------------------------------------------------------------------------------|
| <i>System Parameters &amp; Cost Model</i>             |                                                                                                                                                 |
| $B, B_{\max}$                                         | Current and maximum batch size, where $B \in \{1, \dots, B_{\max}\}$ .                                                                          |
| $\gamma, \Gamma_{\max}$                               | Current and maximum speculative length (draft tokens).                                                                                          |
| $L_{\max}$                                            | Effective skip length, defined as $\max_{1 \leq i \leq B} L_i$ (max lag in a batch).                                                            |
| $C_{\text{switch}}$                                   | Constant representing the KV cache reconstruction cost in the loss function.                                                                    |
| <i>MAB Hierarchical Structure</i>                     |                                                                                                                                                 |
| $t$                                                   | Global decoding time step index.                                                                                                                |
| $j_B$                                                 | Block index for batch size $B$ , governing long-term scheduling scales.                                                                         |
| $b_B$                                                 | Bin index within block $j_B$ , controlling exploration probability ( $p \propto 1/b_B$ ).                                                       |
| $\tau_B$                                              | Round counter within bin $b_B$ .                                                                                                                |
| $H_B$                                                 | Duration of the current block, growing exponentially as $2^{j_B-1}$ .                                                                           |
| <i>Performance Metrics &amp; Regret Analysis</i>      |                                                                                                                                                 |
| $g_{B,\gamma}, \hat{g}_{B,\gamma}$                    | Theoretical goodput (tokens/s) and its empirical mean estimate.                                                                                 |
| $\ell_{B,\gamma}$                                     | Expected latency per token, defined as the inverse goodput ( $1/g_{B,\gamma}$ ).                                                                |
| $\gamma^*$                                            | Optimal speculative length that minimizes the total loss.                                                                                       |
| $L_t(\gamma)$                                         | Realized loss at step $t$ , including latency and switching penalty.                                                                            |
| $R(T)$                                                | Cumulative regret (in terms of latency) over horizon $T$ .                                                                                      |
| <i>Elastic Memory Management</i>                      |                                                                                                                                                 |
| $M_{\text{orig}}, M_{\text{scale}}$                   | Baseline and expanded KV cache memory size (bytes); $M_{\text{scale}} = M_{\text{orig}} + S_{\text{draft}}$ .                                   |
| $S_{\text{draft}}$                                    | Draft model weight memory size (bytes).                                                                                                         |
| $B_{\text{block}}$                                    | Bytes per KV cache block.                                                                                                                       |
| $N_{\text{orig}}, N_{\text{scale}}, N_{\text{draft}}$ | KV cache capacity in blocks: baseline, expanded, and draft-equivalent ( $N_{\text{draft}} = \lceil S_{\text{draft}}/B_{\text{block}} \rceil$ ). |
| $N_{\text{free}}$                                     | Number of currently available physical KV cache blocks.                                                                                         |
| $\tau_{\text{low}}$                                   | Critical scarcity threshold (in blocks) triggering memory expansion.                                                                            |
| $T_{\text{persist}}$                                  | Temporal window size for validating low-memory states.                                                                                          |
| $Q_{\text{wait}}$                                     | Cardinality of the request waiting queue.                                                                                                       |

However, their complexity makes them questionable for latency-sensitive dynamic serving environments. We adopt the relatively simple framework ADA-BINGREEDY proposed in [26]. A key difference between [26] and our approach is that we develop a request batch mechanism to handle varying request patterns, and we design a **loss function** that explicitly considers the speculative length switching cost.

As shown in Figure 5, the Nightjar algorithm adaptively selects the speculative length  $\gamma$  for each batch under continuous batching by organizing time into blocks and bins to balance exploration and exploitation.

To explicitly account for the switching overhead, we reformulate the maximization of goodput into the minimization of latency per token. Formally, at global time  $t$  with batch size  $B$ , the optimal speculative length  $\gamma_t^*$  for an exploitation step is determined by minimizing the regularized latency:

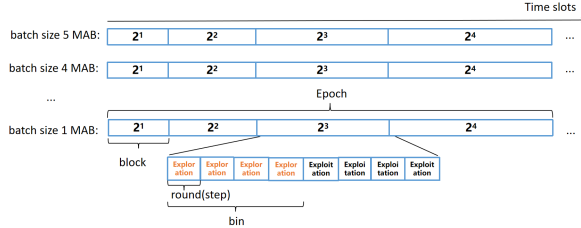


Figure 5. Illustration of the Nightjar algorithm’s three-level hierarchy. Each batch size maintains its own **Epoch**. Each epoch contains **Blocks** ( $j_B$ ) of exponentially growing duration, which are responsible for the long-term schedule. These blocks are further divided into fixed-size **Bins** ( $b_B$ ), the basic units for controlling the exploration-exploitation trade-off. Each **round** ( $\tau_B$ ) is a decoding step.

$$\gamma_t^* = \arg \min_{\gamma \in \{0, 1, \dots, \Gamma_{\max}\}} \left\{ \frac{1}{\tilde{g}_{B,\gamma}} + \frac{\mathbb{I}(\gamma_{t-1} = 0 \wedge \gamma > 0) \cdot C_{\text{switch}}}{\gamma} \right\} \quad (4)$$

Here, we directly estimate the empirical mean latency per token  $\tilde{\ell}_{B,\gamma}$  to avoid bias from Jensen’s inequality ( $\mathbb{E}[1/g] \geq 1/\mathbb{E}[g]$ ). Upon observing the instantaneous latency  $\ell_t = 1/g_t$ , the statistic is updated iteratively via  $\tilde{\ell}_{B,\gamma}^{(n)} \leftarrow \tilde{\ell}_{B,\gamma}^{(n-1)} + \frac{1}{n}(\ell_t - \tilde{\ell}_{B,\gamma}^{(n-1)})$ .

The second term functions as a regularization mechanism for the switching cost.  $\gamma_{t-1}$  is the speculative length at the previous time step. The indicator function  $\mathbb{I}(\cdot)$  activates only when the system transitions from a disabled state ( $\gamma_{t-1} = 0$ ) to an enabled state ( $\gamma > 0$ ), incurring a KV cache reconstruction cost  $C_{\text{switch}}$ . By dividing this cost by  $\gamma$ , the objective favors configurations that amortize the startup overhead across longer speculative sequences, thereby discouraging short-sighted switching that degrades system latency.

Algorithm 1 details the execution flow. To handle the asynchronous nature of continuous batching, Nightjar maintains independent state variables for each batch size  $B$ , organizing time into a hierarchical structure of *blocks* (indexed by  $j_B$ ) and *bins* (indexed by  $b_B$ ).

**Initialization and Bin Selection.** For every time step  $t$ , the algorithm identifies the current batch size  $B$ . Critical decision-making occurs at the onset of a new bin (when the round counter  $\tau_B = 1$ ). At this step, the algorithm determines the bin type: it is designated as an *exploration* bin with probability  $1/b_B$  and as an *exploitation* bin otherwise. This decaying exploration probability ensures aggressive exploration in early stages and progressive convergence to the optimal policy as  $b_B$  increases.

**Arm Selection and Execution.** Upon initializing the bin ( $\tau_B = 1$ ), the speculative length  $\gamma$  is selected and locked for the entire duration of the bin. If it is an exploration bin,  $\gamma$  is sampled uniformly from the available search space to ensure coverage (Lines 10–12). Conversely, in an exploitation bin, the algorithm selects the optimal  $\gamma$  by solving Eq. (4) (Lines 13–15). For all subsequent steps within the bin, the system executes this fixed  $\gamma$ , observes the realized

goodput  $g_t$ , and updates the internal counters. This locking mechanism is essential for bounding the switching cost.

A key feature of Nightjar is its exponential time scaling. A bin concludes when the round counter  $\tau_B$  exceeds  $\sqrt{H_B}$ , and a block concludes when the bin counter  $b_B$  exceeds  $\sqrt{H_B}$  (Lines 20–25). Upon the completion of a block, the block size is updated via  $H_B \leftarrow 2^{j_B-1}$ . This exponential growth ensures that as the history length  $j_B$  increases, the duration of stable exploitation phases grows significantly, allowing the system to capitalize on refined goodput estimates.

**Prefill Cost Modeling.** The effectiveness of Eq. (4) relies on an accurate estimation of  $C_{\text{switch}}$ , which represents the KV cache reconstruction latency. This cost is not static; it varies based on the hardware state and the synchronization gap between the draft and target models.

TABLE 3. MEASURED SWITCHING COST ( $C_{\text{switch}}$ ) ACROSS VARYING BATCH SIZES AND INPUT LENGTHS USING A 7B MODEL ON AN NVIDIA RTX 4090.

| Input Length | Batch Size | $C_{\text{switch}}$ (ms) |
|--------------|------------|--------------------------|
| 128          | 32         | 17.87                    |
| 128          | 64         | 28.53                    |
| 256          | 32         | 20.65                    |
| 256          | 64         | 22.33                    |
| 512          | 32         | 24.30                    |
| 512          | 64         | 102.03                   |

We quantify this overhead using the *effective skip length*, defined as  $L_{\max} = \max\{L_1, \dots, L_B\}$ , where  $L_i$  is the number of new tokens for request  $i$ . The algorithm queries an offline-populated lookup table  $C_{\text{switch}}(L_{\max}, B)$  (Table 3) to obtain the precise cost. To construct this table, we performed offline profiling across a grid of input lengths and geometrically increasing batch sizes (e.g., 2, 4, 8, ...). Specifically, we recorded the prefill time for the standalone target model ( $T_{\text{base}}$ ) and the prefill time with speculative decoding enabled ( $T_{\text{SD}}$ ). The switching cost is derived from the difference  $C_{\text{switch}} = T_{\text{SD}} - T_{\text{base}}$ . As shown in Table 3, on an RTX 4090 setup, this cost can range from 17.87 ms to over 102.03 ms, making dynamic retrieval essential.

**Overhead.** The arm selection execution time is approximately  $1e-5$  seconds, while the average generation time per token in the LLM is 0.034 seconds, a difference of nearly 3400 times. This minimal overhead demonstrates the exceptional efficiency of our method, as the cost of dynamic arm selection is negligible compared to the intrinsic latency of token generation.

## 5. Theoretical Analysis of Regret Bound

In this section, we provide a theoretical analysis of the cumulative regret for the proposed Nightjar algorithm. We demonstrate that the hierarchical bin-based structure effectively controls the switching cost, ensuring sublinear regret.

---

**Algorithm 1:** Nightjar Algorithm

---

**Input** : Max speculative length  $\Gamma_{\max}$ , Max batch size  $B_{\max}$

**Initialize:** Global time  $t \leftarrow 1$

```
1 for  $B = 1$  to  $B_{\max}$  do
2   // Initialize per-batch hierarchy states
3    $j_B \leftarrow 1, H_B \leftarrow 1, b_B \leftarrow 1, \tau_B \leftarrow 1$ 
4 for each time step  $t = 1, 2, \dots$  do
5   Receive current batch size  $B = B_t$ 
6   if  $\tau_B = 1$  then
7     // Bin Start: Select Strategy & Arm
8     Let  $p = 1/b_B$ 
9     Sample  $u \sim \text{Uniform}(0, 1)$ 
10    if  $u < p$  then
11      // Exploration: Random Arm
12       $\gamma_{\text{curr}} \sim \text{Uniform}(\{0, \dots, \Gamma_{\max}\})$ 
13    else
14      // Exploitation: Best Arm (Lock for Bin)
15       $\gamma_{\text{curr}} \leftarrow \text{Eq. (4)}$ 
16    // Execute the locked arm for this step
17    Play  $\gamma_t \leftarrow \gamma_{\text{curr}}$ 
18    Observe goodput  $g_t$  and update  $\tilde{g}_{B, \gamma_t}$ 
19     $\tau_B \leftarrow \tau_B + 1$ 
20    if  $\tau_B > \sqrt{H_B}$  then
21      // Bin Completed
22       $b_B \leftarrow b_B + 1, \tau_B \leftarrow 1$ 
23      if  $b_B > \sqrt{H_B}$  then
24        // Block Completed
25         $j_B \leftarrow j_B + 1, H_B \leftarrow 2^{j_B - 1}, b_B \leftarrow 1$ 
26     $t \leftarrow t + 1$ 
```

---

### 5.1. Preliminaries and Loss Formulation

Unlike standard Multi-Armed Bandit (MAB) settings that maximize reward, Nightjar minimizes the latency per token. Let  $\ell_{B, \gamma} = 1/g_{B, \gamma}$  denote the expected latency per token for a given batch size  $B$  and speculative length  $\gamma$ . We define the switching cost (KV cache reconstruction overhead) as  $C_{\text{switch}}$ .

We formulate the *Loss* at time step  $t$  as:

$$L_t(\gamma_t) = \ell_{B_t, \gamma_t} + \mathbb{I}(\gamma_{t-1} = 0 \wedge \gamma_t > 0) \cdot \frac{C_{\text{switch}}}{\gamma_t} \quad (5)$$

where the second term represents the switching latency amortized over the generated tokens.

The **Cumulative Regret**  $R(T)$  over a time horizon  $T$  is defined as the difference between the total loss incurred by the algorithm and the loss of the optimal fixed policy  $\pi^*$  (which knows the true distributions):

$$R(T) = \sum_{t=1}^T (L_t(\gamma_t) - L_t(\gamma^*)) \quad (6)$$

where  $\gamma^* = \arg \min_{\gamma} \mathbb{E}[\ell_{B, \gamma}]$ .

### 5.2. Upper Bound on Switching Cost

A critical challenge in dynamic speculative decoding is that frequent changes in  $\gamma$  incur high  $C_{\text{switch}}$  costs. Nightjar mitigates this via the **Bin Locking Mechanism**, where the selected arm  $\gamma$  is fixed for the duration of a bin.

**Lemma 1** (Bound on Number of Switches). *The total number of strategy switches  $S_T$  up to time  $T$  is bounded by the number of bins initiated by the algorithm. Consequently, the cumulative switching cost is bounded by  $\mathcal{O}(\sqrt{T})$ .*

*Proof.* In Nightjar, the speculative length  $\gamma$  is re-evaluated only at the start of a bin (when  $\tau_B = 1$ ). Within a bin, the arm remains constant. The algorithm organizes time into blocks indexed by  $j$ . For a block  $j$ , the duration is  $H_j = 2^{j-1}$ , and the bin size is set to  $\sqrt{H_j}$ . The number of bins in block  $j$  is thus  $\sqrt{H_j}$ .

Summing over all blocks up to time  $T$ , the total number of switches  $S_T$  is bounded by:

$$S_T \leq \sum_{j=1}^{\log_2 T} \sqrt{2^{j-1}} \approx \sum_{j=1}^{\log_2 T} 2^{(j-1)/2} = \mathcal{O}(\sqrt{T}) \quad (7)$$

Thus, the total cumulative switching cost is:

$$\text{Cost}_{\text{switch}}(T) \leq S_T \cdot C_{\max} = \mathcal{O}(C_{\max} \sqrt{T}) \quad (8)$$

This ensures that the switching cost component of the regret remains sublinear, preventing the linear regret scenario caused by thrashing.  $\square$

### 5.3. Regret Decomposition and Bound

We decompose the remaining regret (excluding switching costs) into exploration and exploitation components. Our analysis adapts the framework of ADA-BINGREEDY.

**Theorem 1** (Regret Bound). *Assuming a stationary environment where the latency distributions for each batch size  $B$  do not change over time, and by setting the exploration probability  $p_{b_B} \propto 1/b_B$ , the Nightjar algorithm achieves a cumulative regret of:*

$$R(T) = \tilde{\mathcal{O}}(\sqrt{T}) \quad (9)$$

The regret is composed of switching costs and sampling regret (exploration and estimation error).

- 1) **Switching Cost:** From Lemma 1, the number of switches is bounded by the number of bins. Since the bin size scales with  $\sqrt{H_B}$ , the total switching cost is bounded by  $\mathcal{O}(\sqrt{T})$ .
- 2) **Exploration Regret:** With the updated exploration probability  $p = 1/b_B$ , the expected number of exploration bins in a block of duration  $H$  (containing  $K = \sqrt{H}$  bins) is  $\sum_{b=1}^K \frac{1}{b} \approx \ln K$ . Since each bin

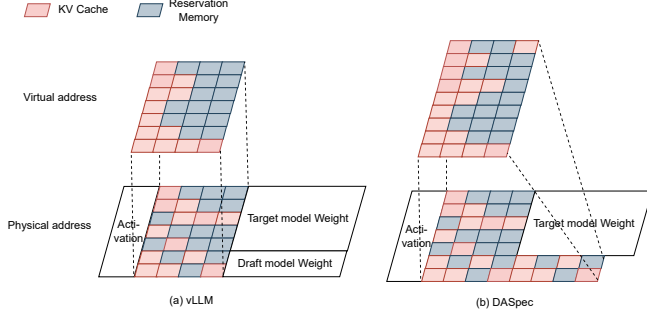


Figure 6. (a) vLLM mitigates memory fragmentation via KV cache virtualization but spatially isolates activation values from the KV cache. (b) Nightjar logically decouples KV cache management from model weights while consolidating them into a unified physical memory pool to maximize utilization.

has duration  $\sqrt{H}$ , the regret incurred by random exploration in this block is  $\mathcal{O}(\sqrt{H} \ln \sqrt{H})$ . Summing over all blocks up to  $T$  yields  $\sum_j \sqrt{2^j} j \approx \tilde{\mathcal{O}}(\sqrt{T})$ .

- 3) **Exploitation Regret:** In exploitation bins, we select the arm with the best empirical regularized latency. Using standard concentration inequalities (e.g., Hoeffding-Azuma), the probability of selecting a suboptimal arm decays exponentially with the number of samples. The analysis follows standard "Batched Bandit" techniques [27], showing that the exploitation regret is dominated by the exploration and switching terms.

Combining these terms, the total regret is  $R(T) = \tilde{\mathcal{O}}(\sqrt{T})$ .

We provide a complete proof in Appendix A.

## 6. Elastic Memory Management for Model-Based Draft Models

Under high system contention, characterized by a backlog in the request queue, the scarcity of KV cache memory often necessitates frequent swap operations or the rejection of active requests. In such saturation regimes, speculative decoding becomes counter-productive due to scheduling overheads. To address this, we propose a dynamic offloading mechanism for model-based draft models. As illustrated in Figure 6, we offload the draft model weights to the host memory, analogous to LoRA adapter management, thereby reclaiming GPU memory to expand the capacity of the original KV cache. We measure both KV cache and draft model in *memory size (bytes)* for unit consistency. Let  $M_{\text{orig}}$  denote the baseline KV cache memory size (bytes); the expanded memory size is  $M_{\text{scale}} = M_{\text{orig}} + S_{\text{draft}}$ , where  $S_{\text{draft}}$  is the draft model weight memory size (bytes). Equivalently, in block count:  $N_{\text{scale}} = N_{\text{orig}} + N_{\text{draft}}$  with  $N_{\text{draft}} = \lceil S_{\text{draft}}/B_{\text{block}} \rceil$  and  $B_{\text{block}}$  the bytes per KV cache block.

### 6.1. Trigger Conditions for Dynamic Adjustment

The system employs an elasticity policy based on real-time metrics of KV cache occupancy and queue depth. A **KV cache expansion** event is triggered when the following conditions converge: (1) Speculative decoding is disabled; (2) The number of available memory blocks, denoted as  $N_{\text{free}}$ , falls below a critical threshold  $\tau_{\text{low}}$  ( $N_{\text{free}} < \tau_{\text{low}}$ ); (3) This resource scarcity persists for a temporal window of  $T_{\text{persist}}$  scheduling steps.

Conversely, a **KV cache contraction** is initiated to restore the draft model when: (1) The waiting queue is empty ( $|Q_{\text{wait}}| = 0$ ); (2) Sufficient free blocks exist to accommodate both the draft model and a safety buffer ( $N_{\text{free}} > N_{\text{draft}} + \tau_{\text{low}}$ ). This hysteresis design ensures that speculative decoding remains disabled during high-load phases (where  $N_{\text{free}} < \tau_{\text{low}}$ ), thereby preventing resource thrashing.

### 6.2. Mechanism of KV Cache Expansion

Upon triggering expansion, the system dynamically reallocates GPU memory. The Model Executor allocates a contiguous memory segment of size  $S_{\text{draft}}$  to the KV cache pool. Subsequently, the Block Manager updates its internal state: (1) The set of allocatable physical block indices is expanded to include the new range  $[K_{\text{boundary}}, K_{\text{total}}]$ ; (2) Reference counters for these newly instantiated blocks are initialized to zero; (3) The new block indices are appended to the free block queue. Crucially, this process is implemented via in-place expansion, eliminating the need for massive memory copying and minimizing reconfiguration overhead.

### 6.3. KV Cache Contraction and Logical Remapping

Contraction is the most critical phase, requiring the compaction of the physical memory layout without compromising active contexts. As depicted in Figure 7, the process involves four sequential steps:

**Step 1: Identification of Eviction Candidates.** The system scans the page tables of all active sequences to identify the set of physical blocks  $\mathcal{B}_{\text{evict}}$  located in the memory region to be reclaimed (i.e., blocks with  $\text{ID} \geq K_{\text{boundary}}$ ). These blocks must be migrated to the preserved memory region  $[0, K_{\text{boundary}}]$ .

**Step 2: Construction of Migration Plan.** The system verifies that the free list contains a sufficient number of slots whose physical block IDs are strictly less than  $K_{\text{boundary}}$ . A one-to-one mapping  $\mathcal{M} : b_{\text{old}} \rightarrow b_{\text{new}}$  is then constructed, assigning each block in  $\mathcal{B}_{\text{evict}}$  to an available slot in the preserved region  $[0, K_{\text{boundary}}]$ . This mapping serves as the basis for the subsequent metadata update and data migration phases.

**Step 3: Metadata Update and Remapping.** For each block requiring migration, the system performs atomic metadata updates: (a) A new physical block object is instantiated,

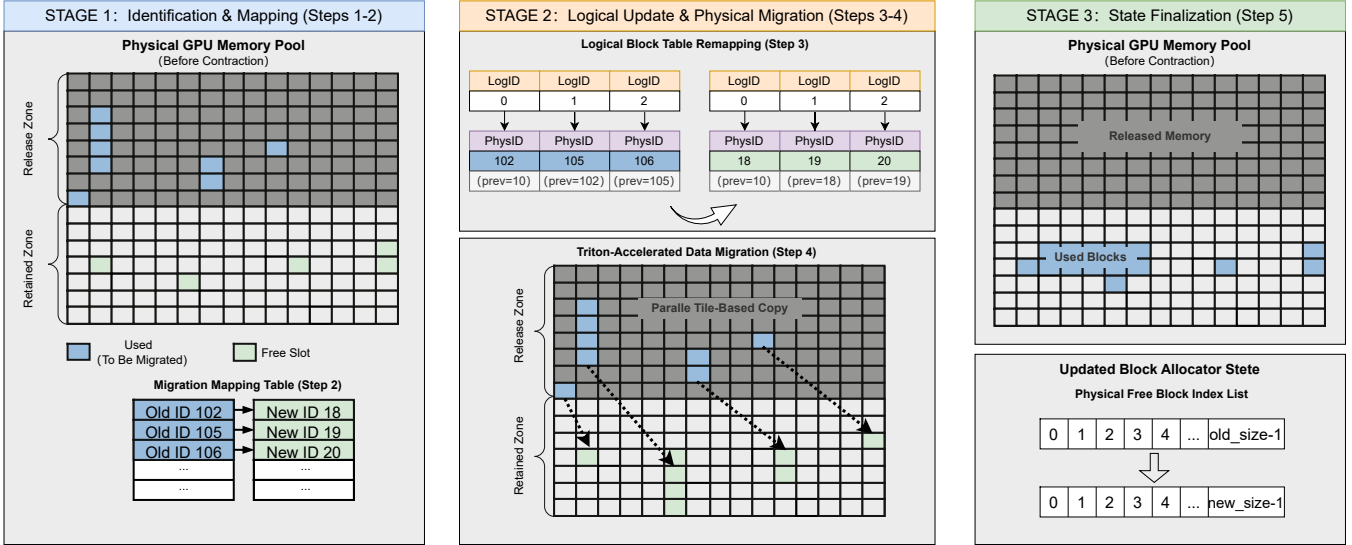


Figure 7. Overview of the KV Cache Block Contraction and Logical Table Remapping process. The system ensures data consistency during physical memory compaction through vectorized data migration.

inheriting the token sequence and size of the original; (b) Predecessor pointers are updated, if a predecessor block is also part of the migration set, the pointer is redirected to its new location; otherwise, the original reference is maintained; (c) The logical Block Table is updated to map the sequence to the new physical block ID; (d) The reference counter for the new block is incremented, and it is marked as allocated. Finally, the old physical block is released, ensuring the logical sequence remains consistent with the physical memory state.

**Step 4: Vectorized Data Migration.** Following the metadata update, the physical data transfer is executed according to the mapping  $\mathcal{M}$ . The migration is powered by a custom high-performance kernel (implemented in Triton) utilizing a tile-based parallelization strategy. Each thread block manages the transfer of a complete KV cache block via vectorized load/store instructions. This approach provides robust performance even on hardware lacking advanced virtual memory management (VMM) features like `cuMemMap`. By decoupling memory reclamation from model execution, we eliminate deadlock risks associated with "hold-and-wait" patterns.

**Step 5: Allocator State Finalization.** Post-migration, the block allocator trims its index set, removing IDs  $\geq K_{\text{boundary}}$  and clearing associated reference counts, effectively finalizing the contraction.

## 6.4. Non-blocking Asynchronous Migration

To minimize latency, we leverage the fact that speculative decoding is inactive during the unloading phase. Consequently, draft model weights are evicted from the GPU immediately, with a backup retained in host memory. Conversely, when memory availability indicates a low re-

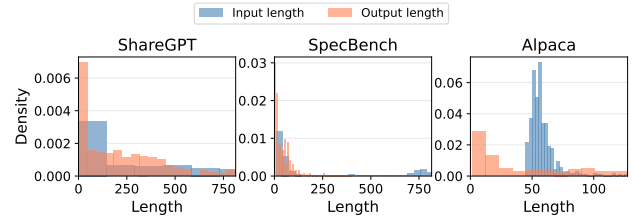


Figure 8. Distribution of Input and Output Lengths Across Three Datasets.

quest rate, the draft model is reloaded to resume accelerated generation. This reloading process utilizes asynchronous CUDA streams with non-blocking Direct Memory Access (DMA). This allows data transfer to overlap with ongoing computation, ensuring that the background management of model weights incurs negligible impact on the serving latency of the primary model.

## 7. Experiments

### 7.1. Experiment setup

**Settings.** We select DeepSeek-R1-Distill-Qwen-7B [28] and Vicuna-13b [29] as target models and match them with DeepSeek-R1-DRAFT-Qwen2.5-0.5B [19] and vicuna-68m [30] as draft models respectively. The model pair for the 7B target model is operated on a single RTX 4090 (24GB) GPU, and the model pair for the 13B target model operates on an A100 (40GB) GPU. Nightjar is implemented by extending the vLLM (version 0.8.2) [4].

**Workloads.** To simulate a dynamic user environment, we generate request arrivals using a Poisson distribution. We also selected real-world production traces from the

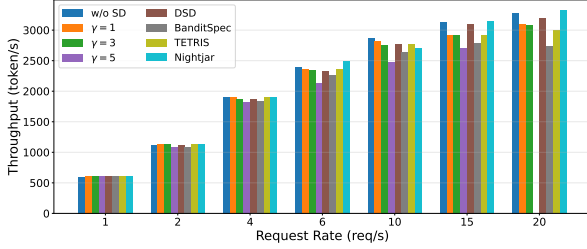


Figure 9. Method Comparison at Low Request Rate and High Request Rate for 7B model.

AzureLLMInferenceDataset [31], and chose a segment with dynamic request rates as shown in Figure 10. For online chatting, we utilize datasets from ShareGPT [32], Alpaca [33]. For other tasks, we utilize SpecBench [1], which is composed of 480 randomly selected instances from six widely used databases. For each dataset, we use 480 instances. The input and output length distribution is presented in Figure 8.

**Baselines.** We evaluate the total token throughput (tokens/s) and mean end-to-end latency of Nightjar against baseline methods:

- **Standard Speculative Decoding (SD):** Implemented on top of vLLM, this baseline employs a vanilla chain-style draft generation (e.g.,  $\gamma = 3$ ), where the draft model generates a sequence of candidate tokens followed by parallel verification from the target model.
- **Vanilla Decoding (w/o SD):** This baseline does not use speculative decoding, where the target model directly generates the response tokens without using the draft model.
- **Dynamic Speculative Decoding (DSD) [13]:** This method utilizes a linear regression model to predict execution latency and estimates the expected acceptance rate based on historical statistics. It dynamically selects the speculative length that maximizes the system *goodput*, defined as the ratio of the expected number of accepted tokens (accepted length +1) to the execution time.
- **BanditSpec [12]:** This approach treats the selection of speculative length as a Multi-Armed Bandit (MAB) problem, leveraging a variant of the Upper Confidence Bound (UCB) algorithm for optimization. However, it does not explicitly incorporate batch size as a contextual feature in its decision-making process.
- **TETRIS [16]:** Given a fixed speculative length (similar to standard SD), TETRIS keeps the draft generation process intact but re-engineers the verification phase. Within a predefined computational budget, it prioritizes the verification of tokens with the highest predictive entropy across a batch to improve verification efficiency.

Our result is averaged over 5 independent runs.

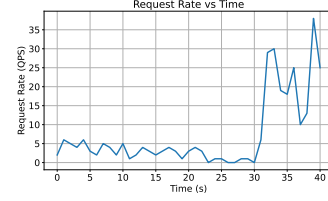


Figure 10. Request Rate Trace.

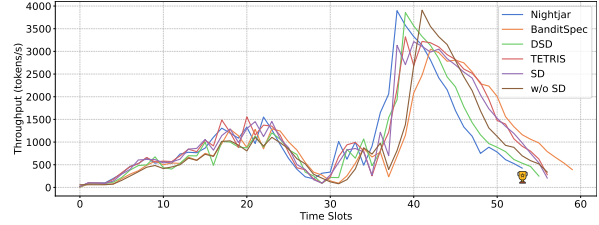


Figure 11. Throughput Trace for 7B model under dynamic request rate.

Nightjar demonstrates robust performance across varying load conditions by dynamically adapting its speculation strategy. As shown in Figure 9, in the detailed breakdown by request rate on ShareGPT dataset, under low request rates (Request Rate  $\leq 4$ ) where speculative decoding outperforms standard decoding, Nightjar maximizes efficiency by selecting the optimal draft length. Conversely, in high request rate scenarios where the overhead of SD renders it inferior to the baseline, Nightjar adaptively disables speculation to avoid performance degradation, thereby consistently achieving superior results in both regimes. Note that data for  $\gamma = 5$  at 20 QPS is excluded from Figure 9 owing to GPU memory limitations.

## 7.2. Dynamic request load

For 7B model under dynamic request rate (Figure 10), as shown in Figure 11, During low request load periods, Nightjar achieves the highest peak throughput by dynamically selecting the optimal speculative length. Conversely, during high-load phases, it strategically disables speculation to revert to standard vanilla decoding. This prevents the severe performance degradation that plagues other speculative methods, allowing Nightjar to maintain consistently superior overall throughput across varying traffic conditions. DSD’s predictions are less accurate during low request load, leading to throughput degradation, but perform better under high request load, while TETRIS exhibits performance drops under high request load due to its high overhead in large batch size and static BanditSpec is not suitable for dynamic batch size.

As summarized in Table 4, Nightjar demonstrates superior performance across all evaluated scenarios. Compared to standard auto-regressive decoding (w/o SD), our method yields a substantial average throughput increase of 27.29%. More importantly, when compared against highly optimized speculative decoding baselines, Nightjar still maintains a

TABLE 4. THROUGHPUT (TOKENS/S) COMPARISON FOR 7B AND 13B MODELS

| Method     | 7B      |          |           | 13B    |          |           |
|------------|---------|----------|-----------|--------|----------|-----------|
|            | Alpaca  | ShareGPT | SpecBench | Alpaca | ShareGPT | SpecBench |
| Nightjar   | 2102.73 | 3734.23  | 3326.20   | 721.23 | 1729.68  | 1061.82   |
| BanditSpec | 1860.74 | 3428.75  | 2631.43   | 679.82 | 1383.81  | 763.15    |
| DSD        | 2044.40 | 3614.65  | 2789.51   | 603.32 | 1244.96  | 692.01    |
| TETRIS     | 1875.91 | 3597.21  | 2974.14   | 702.65 | 1628.86  | 985.40    |
| SD         | 1920.63 | 3593.36  | 3044.80   | 628.47 | 1689.53  | 964.02    |
| w/o SD     | 2072.38 | 3653.61  | 3207.28   | 438.13 | 1290.04  | 673.48    |

TABLE 5. MEAN END-TO-END LATENCY (MS) COMPARISON FOR 7B AND 13B MODELS

| Method     | 7B       |          |           | 13B      |          |           |
|------------|----------|----------|-----------|----------|----------|-----------|
|            | Alpaca   | ShareGPT | SpecBench | Alpaca   | ShareGPT | SpecBench |
| Nightjar   | 8868.17  | 6534.76  | 7618.85   | 23525.49 | 8133.92  | 14691.81  |
| BanditSpec | 12340.83 | 7799.63  | 9288.23   | 29077.32 | 9667.04  | 19294.42  |
| DSD        | 9183.21  | 6499.12  | 8301.02   | 16212.44 | 10057.72 | 22361.71  |
| TETRIS     | 11734.19 | 7409.62  | 8789.48   | 22133.43 | 8046.25  | 14937.37  |
| SD         | 11110.68 | 7047.49  | 8567.04   | 24671.40 | 8152.97  | 14212.97  |
| w/o SD     | 8876.14  | 6438.47  | 7654.05   | 32222.49 | 9350.87  | 23831.74  |

clear edge. Specifically, it surpasses DSD and BanditSpec by 22.89% and 19.76% on average, respectively. Even against the strongest baselines, TETRIS and SD, Nightjar achieves competitive average improvements of 7.39% and 8.32%, proving the effectiveness of our proposed design.

Compared to the vanilla auto-regressive baseline (w/o SD), Nightjar achieves an average end-to-end latency reduction of 12.90%. Notably, the performance gains are highly correlated with the target model size. On the 7B model, the latency remains comparable to the baseline, primarily because the overhead of draft token generation and verification offsets the speculative benefits when the base generation speed is already high. However, on the 13B model, where generation costs are significantly heavier, Nightjar demonstrates exceptional efficiency, reducing end-to-end latency by up to 38.35% (on SpecBench).

### 7.3. Ablation and Analysis

**7.3.1. Context-Aware Bandit Methods.** We conduct ablation experiments on 7B model. Figure 12 additionally compares various context-aware multi-armed bandit methods (batch size as context) and the basic ADA-BINGREEDY approach. Our method consistently achieves optimal performance across different QPS levels because LinUCB and linearTS assume linear relationships between rewards and contexts, which don’t hold for LLM speculative serving scenarios. Throughput depends not only on hardware but also on acceptance rates and model types, making linear models unsuitable for this complex scenario.

**7.3.2. Efficacy of Dynamic Model Offloading.** For 7B model, the impact of our dynamic loading and unloading mechanism is assessed by comparing Nightjar-Offload with the standard Nightjar implementation. Results in Figure 13 demonstrate that offloading becomes increasingly beneficial as the system enters the compute-bound regime at high request rates, reaching a peak throughput of 6315.9 tok/s at 35 req/s, a substantial improvement over the 5982.6 tok/s achieved without offloading. This confirms that liberating

GPU memory by unloading draft models effectively expands the KV cache capacity for the target model, directly translating to higher service concurrency.

**7.3.3. Sensitivity to Trigger Thresholds.** We further investigate the sensitivity of system performance to the free KV cache threshold  $N_{low}$ , which dictates the timing for dynamic adjustments. Figure 14 illustrates that the system reaches an optimal throughput plateau of approximately 6110 tok/s at a 10% free cache threshold, which significantly exceeds the fixed baseline performance of 5768.12 tok/s. This result indicates that a 10% buffer provides the ideal balance between sustaining speculative decoding and preventing memory exhaustion, ensuring robust QoS under heavy traffic conditions.

**7.3.4. Compare with different speculative length.** As shown in Figure 15, when compared against the best-performing fixed speculative lengths (such as  $\gamma = 2$  or  $\gamma = 4$  at their peak efficiency) for 13B model, Nightjar consistently maintains a 1% to 16% performance advantage. This demonstrates exceptional robustness, as Nightjar never falls behind the optimal static configuration.

**7.3.5. Scalability Analysis on Multi-GPU Settings.** In this experiment, we deploy a 30B-scale model across two NVIDIA L20 (48GB) GPUs using tensor parallelism. Specifically, we use Qwen2.5-32B-Instruct as the target model and Qwen2.5-0.5B-Instruct as the draft model. As shown in Figure 16, by comparing Nightjar against other baselines, we observe that Nightjar maintains its performance advantage even when scaling to larger models distributed across multiple GPUs.

TABLE 6. OVERHEAD OF ELASTIC MEMORY OPERATIONS FOR 30B MODEL ON 2 L20 GPUS.

| Operation                                       | Latency      |
|-------------------------------------------------|--------------|
| KV Cache Block Expansion                        | 143.9 ms     |
| KV Cache Block Contraction (Triton-accelerated) | 11.9 ms      |
| Draft Model Reload Dispatch (CPU Overhead)      | 21.9 $\mu$ s |

**7.3.6. Overhead of Elastic Memory Operations.** As shown in Table 6, we further quantified the overhead of these dynamic adjustments to ensure they do not disrupt real-time serving for 30B model on 2 L20 GPUs. The KV cache contraction process, accelerated by our custom Triton kernel, completes in just 11.9 ms, allowing for rapid memory reclamation during load spikes. Conversely, KV cache expansion takes 143.9 ms, a simplified cost acceptable during the transition to low-load states. Notably, triggering the draft model reload incurs a negligible CPU overhead of only 21.9  $\mu$ s, confirming that our non-blocking asynchronous stream management effectively hides the data transfer latency from the critical scheduling path.

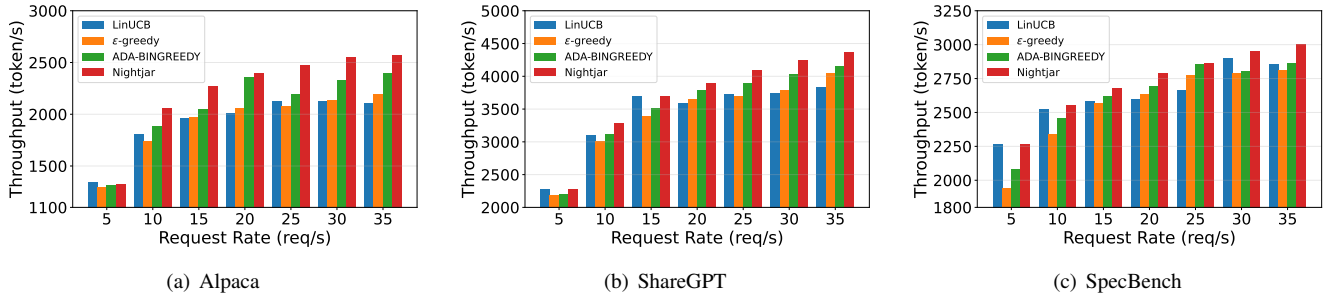


Figure 12. Context-aware bandit method comparison on Alpaca, ShareGPT and SpecBench datasets.

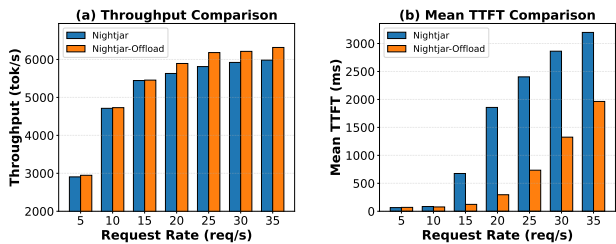


Figure 13. Performance Comparison of with offload and without offload

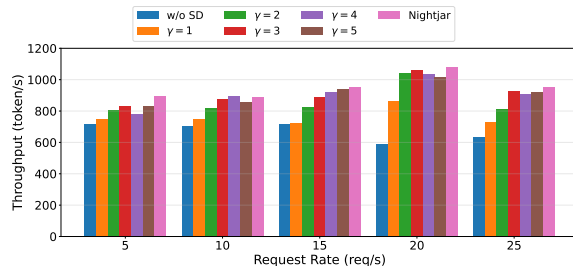


Figure 15. Throughput comparison for static request rate on SpecBench dataset. Comparison among different speculative length  $\gamma$  for 13B model.

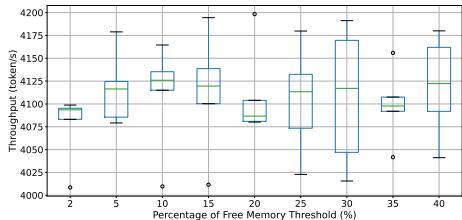


Figure 14. Performance Comparison of with different thresholds

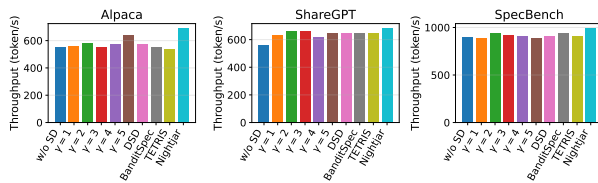


Figure 16. Performance Comparison of 30B model

## 8. Related Work

### 8.1. Speculative Decoding in LLM Serving

While various approaches have sought to optimize speculative decoding, they often fail to address the dynamic and unpredictable nature of real-world LLM serving loads. Initial efforts focused on single-request optimization [6], [7], [8], [9], [10] or static offline batches [11], [12], employing predictive algorithms [7] or confidence-based methods [14], [6], [16], but their static nature makes them fundamentally ill-suited for the fluctuating request rates in live environments. More recent works have explored dynamic speculation length adjustment in serving systems [11], [13], [14], [15], yet they exhibit significant limitations. For instance, SpecServe [14] and TETRIS [16] rely on draft confidence scores, but this can lead to poor performance with large batch sizes and still requires generating at least one token. DSD [13] optimizes length via linear goodput modeling, but its reliance on past average acceptance rates introduces a critical vulnerability. This dependency on historical data, found in methods like DSD [13] and SpecServe [14], can lead to a “decision deadlock” where disabling speculative

decoding permanently halts the collection of new acceptance rate data, locking the system in a suboptimal state. Our exploration-exploitation approach is designed to mitigate this risk. Although BanditSpec [12] introduces a Multi-Armed Bandit (MAB) paradigm, it is constrained by its static design, rendering it incompatible with the continuous batching [4] of modern serving systems. Furthermore, to the best of our knowledge, existing works largely overlook the “switching cost” incurred when re-enabling speculative decoding from a length of 0, which is the overhead of KV cache reconstruction for the draft model.

### 8.2. Unified Memory Management for Weights and KV Cache in LLM Serving

Oneiros [17] targets multi-model deployment by introducing a dynamic memory remapping engine that redirects GPU memory reserved for model parameters to the KV cache. Unlike Nightjar, which completely unloads draft model weights when they are not in use, Oneiros operates on active models. By performing remapping at layer gran-

ularity, it enables models to remain in a serving state while utilizing asynchronous transfers to fetch required parameters in real-time before execution. This approach effectively hides latency by overlapping computation with parameter transfer. eLLM [18] focuses on intra-model efficiency, enabling the KV cache and activation tensors to borrow space from a shared physical memory pool, effectively breaking the traditional isolation between these resources. FineServe [34] provides a unified management framework for both weights and KV caches across multiple models, specifically addressing the challenges of serving models with heterogeneous quantization precisions. While these works optimize memory sharing for active models or intra-model tensors, they do not address the unique memory bottlenecks associated with dynamically swapping draft model weights in speculative decoding, a gap our work aims to fill.

## 9. Conclusions

In this paper, we presented Nightjar, an innovative learning-based algorithm for optimizing speculative decoding. By modeling the speculative length selection as a multi-armed bandit problem, Nightjar dynamically chooses the best decoding strategy for different batch sizes, maximizing throughput and minimizing latency. Extensive evaluations confirm that Nightjar provides superior performance, highlighting a promising direction for more efficient and responsive LLM serving solutions.

## References

- [1] H. Xia, Z. Yang, Q. Dong, P. Wang, Y. Li, T. Ge, T. Liu, W. Li, and Z. Sui, "Unlocking efficiency in large language model inference: A comprehensive survey of speculative decoding," in *Findings of the Association for Computational Linguistics ACL 2024*, Aug. 2024, pp. 7655–7671.
- [2] Y. Leviathan, M. Kalman, and Y. Matias, "Fast inference from transformers via speculative decoding," in *International Conference on Machine Learning*. PMLR, 2023, pp. 19274–19286.
- [3] L. Zhang, Z. Zhang, R. Li, Z. Tian, S. Mei, D. Li *et al.*, "Dovetail: A cpu/gpu heterogeneous speculative decoding for llm inference," in *Proceedings of the 2025 Conference on Empirical Methods in Natural Language Processing*, 2025, pp. 17393–17406.
- [4] W. Kwon, Z. Li, S. Zhuang, Y. Sheng, L. Zheng, C. H. Yu, J. Gonzalez, H. Zhang, and I. Stoica, "Efficient memory management for large language model serving with pagedattention," in *Proceedings of the 29th symposium on operating systems principles*, 2023, pp. 611–626.
- [5] X. Liu, J. Yu, J. Park, I. Stoica, and A. Cheung, "Speculative decoding: Performance or illusion?" *arXiv preprint arXiv:2601.11580*, 2025.
- [6] J. Wang, Y. Su, J. Li, Q. Xia, Z. Ye, X. Duan, Z. Wang, and M. Zhang, "Opt-tree: Speculative decoding with adaptive draft tree structure," *Transactions of the Association for Computational Linguistics*, vol. 13, pp. 188–199, 2025.
- [7] S. Zhang, H. Wang, D. Ma, Z. Zhu, L. Chen, K. Lan, and K. Yu, "Ada eagle: Optimizing speculative decoding via explicit modeling of adaptive draft structures," *arXiv preprint arXiv:2412.18910*, 2024.
- [8] Z. Zhang, J. Xu, T. Liang, X. Chen, Z. He, R. Wang, and Z. Tu, "Draft model knows when to stop: A self-verification length policy for speculative decoding," *arXiv preprint arXiv:2411.18462*, 2024.
- [9] O. Brown, Z. Wang, A. Do, N. Mathew, and C. Yu, "Dynamic depth decoding: Faster speculative decoding for llms," *arXiv preprint arXiv:2409.00142*, 2024.
- [10] K. Huang, X. Guo, and M. Wang, "Specdec++: Boosting speculative decoding via adaptive candidate lengths," *arXiv preprint arXiv:2405.19715*, 2024.
- [11] Q. Su, C. Giannoula, and G. Pekhimenko, "The synergy of speculative decoding and batching in serving large language models," *arXiv preprint arXiv:2310.18813*, 2023.
- [12] Y. Hou, F. Zhang, C. Du, X. Zhang, J. Pan, T. Pang, C. Du, V. Y. Tan, and Z. Yang, "Banditspec: Adaptive speculative decoding via bandit algorithms," *arXiv preprint arXiv:2505.15141*, 2025.
- [13] X. Liu, C. Daniel, L. Hu, W. Kwon, Z. Li, X. Mo, A. Cheung, Z. Deng, I. Stoica, and H. Zhang, "Optimizing speculative decoding for serving large language models using goodput," *arXiv preprint arXiv:2406.14066*, 2024.
- [14] K. Huang, H. Wu, Z. Shi, H. Zou, M. Yu, and Q. Shi, "Specserve: Efficient and slo-aware large language model serving with adaptive speculative decoding," *arXiv preprint arXiv:2503.05096*, 2025.
- [15] Z. Li, Z. Chen, R. Delacourt, G. Oliaro, Z. Wang, Q. Chen, S. Lin, A. Yang, Z. Zhang, Z. Chen *et al.*, "Adaserve: Slo-customized llm serving with fine-grained speculative decoding," *arXiv e-prints*, pp. arXiv–2501, 2025.
- [16] Z. Wu, Z. Zhou, A. Verma, A. Prakash, D. Rus, and B. K. H. Low, "Tetris: Optimal draft token selection for batch speculative decoding," *arXiv preprint arXiv:2502.15197*, 2025.
- [17] R. Li, S. Pal, V. N. Pullu, P. Sinha, J. Ryoo, L. K. John, and N. J. Yadwadkar, "Oneiros: Kv cache optimization through parameter remapping for multi-tenant llm serving," in *Proceedings of the 2025 ACM Symposium on Cloud Computing*, 2025, pp. 88–101.
- [18] J. Xu, R. Zhang, Y. Xiong, C. Guo, Z. Liu, Y. Zhou, W. Hu, H. Wu, C. Shao, Z. Wang *et al.*, "ellm: Elastic memory management framework for efficient llm serving," *arXiv preprint arXiv:2506.15155*, 2025.
- [19] Alamos, "Deepseek-r1-draft-qwen2.5-0.5b," <https://huggingface.co/alamios/DeepSeek-R1-DRAFT-Qwen2.5-0.5B>, 2024, accessed: 2025-03-30.
- [20] R. Sadhukhan, J. Chen, Z. Chen, V. Tiwari, R. Lai, J. Shi, I. E.-H. Yen, A. May, T. Chen, and B. Chen, "Magicdec: Breaking the latency-throughput tradeoff for long context generation with speculative decoding," *arXiv preprint arXiv:2408.11049*, 2024.
- [21] Y. Li, F. Wei, C. Zhang, and H. Zhang, "Eagle-2: Faster inference of language models with dynamic draft trees," *arXiv preprint arXiv:2406.16858*, 2024.
- [22] D. Guo, D. Yang, H. Zhang, J. Song, R. Zhang, R. Xu, Q. Zhu, S. Ma, P. Wang, X. Bi *et al.*, "Deepseek-r1: Incentivizing reasoning capability in llms via reinforcement learning," *arXiv preprint arXiv:2501.12948*, 2025.
- [23] S. Agrawal and N. Goyal, "Thompson sampling for contextual bandits with linear payoffs," in *International conference on machine learning*. PMLR, 2013, pp. 127–135.
- [24] L. Li, W. Chu, J. Langford, and R. E. Schapire, "A contextual-bandit approach to personalized news article recommendation," in *Proceedings of the 19th international conference on World wide web*, 2010, pp. 661–670.
- [25] A. Stolcke, A. Raju, C. Vaz, D. He, V. Ravichandran, V. A. Trinh *et al.*, "Adaptive endpointing with deep contextual multi-armed bandits," in *ICASSP 2023-2023 IEEE International Conference on Acoustics, Speech and Signal Processing (ICASSP)*. IEEE, 2023, pp. 1–5.
- [26] H. Luo, C.-Y. Wei, A. Agarwal, and J. Langford, "Efficient contextual bandits in non-stationary worlds," in *Conference On Learning Theory*. PMLR, 2018, pp. 1739–1776.

- [27] Z. Gao, Y. Han, Z. Ren, and Z. Zhou, “Batched multi-armed bandits problem,” *Advances in Neural Information Processing Systems*, vol. 32, 2019.
- [28] DeepSeek, “Deepseek-r1-distill-qwen-7b,” <https://huggingface.co/deepseek-ai/DeepSeek-R1-Distill-Qwen-7B>, 2024, accessed: 2025-03-20.
- [29] lmsys, “vicuna-13b-v1.5,” Hugging Face Model Hub, accessed: 2025-08-14. [Online]. Available: <https://huggingface.co/lmsys/vicuna-13b-v1.5>
- [30] double7, “vicuna-68m,” Hugging Face Model Hub, accessed: 2025-08-14. [Online]. Available: <https://huggingface.co/double7/vicuna-68m>
- [31] M. Azure, “Azure public dataset,” <https://github.com/Azure/AzurePublicDataset>, 2023, accessed: 2025-03-20.
- [32] anon8231489123, “Sharegpt\_v3\_unfiltered\_cleaned\_split\_no\_imsorry.json,” [https://huggingface.co/datasets/anon8231489123/ShareGPT\\_Vicuna\\_unfiltered/blob/main/ShareGPT\\_V3\\_unfiltered\\_cleaned\\_split\\_no\\_imsorry.json](https://huggingface.co/datasets/anon8231489123/ShareGPT_Vicuna_unfiltered/blob/main/ShareGPT_V3_unfiltered_cleaned_split_no_imsorry.json), 2023, accessed: 2025-03-20.
- [33] T. Lab, “Alpaca dataset,” <https://huggingface.co/datasets/tatsu-lab/alpaca>, 2023, accessed: 2025-04-15.
- [34] K. Bin, S. Choi, J. Son, J. Choi, D. Bae, D. Baek, K. Moon, M. Jang, and H. Lee, “Fineserve: Precision-aware kv slab and two-level scheduling for heterogeneous precision llm serving,” *arXiv preprint arXiv:2509.06261*, 2025.

## Appendix

In this appendix, we provide the complete derivation of the regret bound for the Nightjar algorithm. Our objective is to minimize the cumulative latency per token. A key aspect of our formulation is the specific structure of the loss function, which penalizes strategy switches inversely proportional to the speculative length.

### 1. Problem Setup and Definitions

Let  $\mathcal{A} = \{0, 1, \dots, \Gamma_{\max}\}$  be the set of available arms (speculative lengths). At each time step  $t$ , the algorithm selects an arm  $\gamma_t \in \mathcal{A}$ . We define the instantaneous **Loss** observed at step  $t$  as:

$$L_t(\gamma_t) = \ell_{B, \gamma_t} + \mathbb{I}(\gamma_{t-1} = 0 \wedge \gamma_t > 0) \cdot \frac{C_{\text{switch}}}{\gamma_t} \quad (10)$$

where  $\ell_{B, \gamma_t} = 1/g_{B, \gamma_t}$  is the latency per token, and the second term represents the switching overhead amortized by the speculative length  $\gamma_t$ .

The **Cumulative Regret** over horizon  $T$  is defined against an optimal fixed policy  $\gamma^*$  that knows the true distributions:

$$R(T) = \sum_{t=1}^T (L_t(\gamma_t) - L_t(\gamma^*)) \quad (11)$$

Since the optimal policy  $\gamma^*$  is static, it incurs the switching cost at most once (at  $t = 1$ ), which is negligible as  $T \rightarrow \infty$ . Thus, we can decompose the regret into performance regret and switching regret:

$$R(T) \leq \underbrace{\sum_{t=1}^T (\ell_{B, \gamma_t} - \ell_{B, \gamma^*})}_{R_{\text{perf}}(T)} + \underbrace{\sum_{t=1}^T \mathbb{I}(\text{switch}_t) \cdot \frac{C_{\text{switch}}}{\gamma_t}}_{R_{\text{switch}}(T)} \quad (12)$$

### 2. Bound on Switching Cost Regret

We first analyze  $R_{\text{switch}}(T)$ . The specific design of our loss function scales the switching penalty by  $1/\gamma_t$ . Since any valid switch implies  $\gamma_t \geq 1$ , we have the inequality:

$$\frac{C_{\text{switch}}}{\gamma_t} \leq C_{\text{switch}} \quad (13)$$

This implies that the switching cost is bounded by a constant maximum overhead  $C_{\text{max}}$  regardless of the chosen arm.

The Nightjar algorithm employs a *Bin Locking Mechanism*, where the arm  $\gamma_t$  is fixed for the duration of a bin. Therefore, a switch can only occur at the boundary of a bin. Let  $S_T$  be the total number of bins initiated up to time  $T$ . As shown in the algorithm design, the timeline is divided into blocks  $j$  of length  $H_j = 2^{j-1}$ , and each block contains  $K_j \approx \sqrt{H_j}$  bins.

**Lemma 2 (Switching Count Bound).** *The total number of strategy switches is bounded by the number of bins:*

$$N_{\text{bins}} \leq \sum_{j=1}^{\log_2 T} \sqrt{2^{j-1}} = \mathcal{O}(\sqrt{T}) \quad (14)$$

Combining the cost bound and the count bound:

$$R_{\text{switch}}(T) \leq C_{\text{max}} \cdot N_{\text{bins}} = \mathcal{O}(C_{\text{max}} \sqrt{T}) = \tilde{\mathcal{O}}(\sqrt{T}) \quad (15)$$

This confirms that even with the inverse-proportional penalty term, the switching regret remains sublinear.

### 3. Bound on Performance Regret

The analysis for  $R_{\text{perf}}(T)$  follows the standard decomposition into exploration and exploitation phases.

**3.1. Exploration Regret.** In block  $j$ , the algorithm explores with probability  $p_{j,b} \propto 1/b$ , where  $b$  is the bin index. The expected number of exploration bins grows logarithmically with the block size:

$$\mathbb{E}[N_{\text{explore}}^{(j)}] \approx \ln(\sqrt{H_j}) \quad (16)$$

Since each bin has duration  $W_j \approx \sqrt{H_j}$ , the regret from random exploration is:

$$R_{\text{explore}}(T) = \sum_{j=1}^{\log_2 T} \Delta_{\text{max}} \sqrt{H_j} \ln \sqrt{H_j} = \tilde{\mathcal{O}}(\sqrt{T}) \quad (17)$$

**3.2. Exploitation Regret.** In exploitation bins, the algorithm selects the arm that minimizes the empirical estimate of the regularized loss defined in Eq. (10). Using the Hoeffding-Azuma inequality for martingales, the probability of selecting a suboptimal arm decays exponentially with the number of samples collected in previous bins. As established in [26], the exploitation regret is dominated by the exploration and switching terms, bounded by  $\mathcal{O}(\sqrt{T})$ .

## 4. Conclusion

Summing the components:

$$R(T) = \tilde{O}(\sqrt{T}) + \tilde{O}(\sqrt{T}) = \tilde{O}(\sqrt{T}) \quad (18)$$

The Nightjar algorithm achieves sublinear regret, effectively balancing the trade-off between maximizing goodput (minimizing latency) and minimizing the KV cache reconstruction overhead defined by the specific loss function  $C_{\text{switch}}/\gamma$ .